Supplementary Information

Complex lattice occupations of copper leading to enhanced thermoelectric performance in *n*-type PbSe

Yalin Shi,‡[a] Mingkai He,‡[b] Minchao Cui,*[c] Weishuai Wang,[a] Baopeng Ma,[ad] Fudong Zhang,[a] Beiquan Jia,[a] Xiaolian Chao,[a] Zupei Yang,*[a] Di Wu*[a]

[a] Key Laboratory for Macromolecular Science of Shaanxi Province and Shaanxi Key Laboratory for Advanced Energy Devices, School of Materials Science and Engineering, Shaanxi Normal University, Xi'an 710062, China

E-mail: yangzp@snnu.edu.cn, wud@snnu.edu.cn

[b] Beijing Institute of Nanoenergy and Nanosystems, Chinese Academy of Sciences, Beijing 101400, China

[c] Key Laboratory of High Performance Manufacturing for Aero Engine (MIIT) Northwestern Polytechnical University, Xi'an 710072, China

E-mail: cuiminchao@nwpu.edu.cn

[d] School of Materials Science and Engineering and Institute of Materials Genome & Big Data, Harbin Institute of Technology, Shenzhen, 518055, China.

1. Experiments

Sample synthesis

All samples were prepared by high-temperature melting combined with spark plasma sintering technology. For the samples of composition PbSe-x%Cu (x = 0, 0.2, 0.4, 0.6, 0.8 and 1.0), PbSe-y%Cu_2Se (y = 0, 0.5, 1.0, 2.0, 3.0, 5.0), PbSe-3%Cu_2Se-z%Cu (z = 0, 0.4, 0.6, 0.8, 1.0), high-purity raw materials Pb, Se and Cu particles (99.999%, Alfa Aesar, China) were weighed according to stoichiometric ratio and encapsulated into quartz tubes under the residual pressure less than ~ 10^{-4} torr. Then the quartz tubes were placed into muffle furnaces and slowly heated to 450K within 12h, rapidly heated to 1150K in 6 h, kept for 6 h at this temperature and then naturally cooling. Afterwards, the obtained ingots were grinded into powder and then sintered with spark plasma sintering. All samples possessed the same sintering procedure: firstly, the powder was heated to 500℃ at a rate of 100K/min, then slowly heated to 550℃ within 1 min and then soaked for 5 minutes with an axial pressure of 50 MPa. The obtained pellets were cut into the bar-shaped pieces of 12×3×3 mm for electrical transport measurements and a squared shape of 6×6×1.8 mm for thermal diffusivity measurements.

Thermoelectric properties

The electrical conductivity and the Seebeck coefficient of obtained samples were measured simultaneously by a commercial ZEM-3 (Ultravac, Japan) instrument under a low-pressure Helium atmosphere from room temperature to 773 K. The experimental error for each measurement was expected to be within 5%. The thermal conductivity is calculated from the relationship $\kappa_{tot}=D\rho C_p$, where the thermal diffusivity (D) was calculated in N_2 Laser Flash Diffusion Method LFA 467 (Netzsch, Germany) in the temperature range 298K to 773K. The heat capacity (C_p) was calculated from the Dulong-Petit limit law of theory $3NR/\bar{M}$, where $\bar{M}$ is the average atomic mass per mole. Sample density (ρ) was measured using the Archimedes method. The lattice thermal conductivity (κ_{lat}) was calculated by subtracting the electronic thermal conductivity (κ_{ele}), where is related to the electrical conductivity.

Phase and Microstructure Characterizations

X-ray diffraction (PXRD) patterns were recorded from finely ground powders of samples using a XRD diffractor (Rigaku, Japan, Cu-K_α) with radiation operating at 40 kV and 20 mA. The scanning range of 2θ was 20-80° with a scanning speed of 6°/min. Scanning electron

microscope (SEM, SUB8020, Japan) equipped with energy dispersive spectroscopy (EDS) was used to detect its microstructure and corresponding elements distribution at micron-scale level. A FEI Themis Z was used to for the TEM analysis under a voltage of 300 kV.

Hall measurements

The room-temperature carrier concentration was measured using the Van Der Pauw method using a commercial instrument (Lake Shore 8400 series, 58 USA).

2. Theoretical simulations/calculations

Debye-Callaway model

Using the Debye-Callaway model, the final temperature (T)-dependent can be expressed as a sum κ_{lat} (T) of the spectral lattice thermal conductivity from different frequencies:

$$\kappa_{\text{lat}} = \int \kappa_s(\omega) d\omega = \frac{1}{3}\int_0^{\omega_a} C_s(\omega) v_g(\omega)^2 \tau_{tot}(\omega) d\omega \quad (1)$$

Thus, the $\kappa_s(\omega)$ is determined by the $C_s(\omega)$, the frequency-dependent phonon group velocity v_g (ω) and total relaxation time $\kappa_{tot}(\omega)$. Generally, as the phonons in optical branches shows low velocity, only the phonons in acoustic branches are considered to calculate the κ_{lat}. Thus, the cut-off frequency for acoustic branches ω_a is given by $\omega_a = (\frac{6\pi^2}{V_{\text{cell}}})^{1/3}$, $v_s = (\frac{6\pi^2}{NV_{\text{av}}})^{1/3}$ where N, V_{av} and v_s the atomic numbers in a primitive cell, average atomic volume and sound speed respectively. For simple approximation, the frequency-dependent phonon group velocity $v_g(\omega)$ is set as a constant value v_s, and κ_{lat} is calculated by the following equation (2):

$$\kappa_{\text{lat}} = \frac{k_B}{2\pi^2 \upsilon_S}(\frac{k_B}{\hbar})\int_0^{\theta a/T} \tau_{tot}(x) \frac{x^4 e^x}{(e^x - 1)^2} dx \quad (2)$$

$$\theta a = \hbar\omega a / k_B = (\frac{6\pi^2}{NV_{av}})^{1/3} \hbar v_s / k_B \quad (3)$$

The dimensionless variable x in equation (2) is defined as $x = \hbar\omega/k_B T$, where ω is the phonon frequency. The τ_{tot} (x) is the reciprocal sum of the relaxationtimes from different scattering mechanisms according to the Matthiessen's rule:

$$\tau = \tau_U^{-1} + \tau_N^{-1} + \tau_{PD}^{-1} + \tau_B^{-1} + \tau_{NP}^{-1} + \tau_{DC}^{-1} + \tau_{DS}^{-1} \quad (4)$$

where, τ_U^{-1}, τ_N^{-1}, τ_{PD}^{-1}, τ_B^{-1} and τ_{NP}^{-1} are the contributions from the Umklapp phonon-phonon scattering, normal phonon-phonon scattering, point-defect scattering, boundary scattering,

nanoprecipitates scattering and dislocation scattering.

The τ_U^{-1} is calculated from the following equation:

$$\tau_U^{-1} = \frac{2k_B^3 V_{av}^{1/3} \gamma^2 T^3}{(6\pi^2)^{1/3} M_{av} v_s^3 \hbar^2} x^2 \exp(-\frac{\theta_a}{bT}) \quad (5)$$

The τ_N^{-1} is calculated from the following equation:

$$\tau_N^{-1} = B_N \tau_U^{-1} \quad (6)$$

The τ_{PD}^{-1} is calculated from the following equation:

$$\tau_{PD}^{-1} = \frac{V_{av}\Gamma}{4\pi v_s^3} \omega^4 = \frac{V_{av}\Gamma}{4\pi v_s^3} (\frac{k_B T}{\hbar})^4 x^4 \quad (7)$$

The τ_B^{-1} is calculated from the following equation:

$$\tau_B^{-1} = \frac{vs}{D} \quad (8)$$

The τ_{NP}^{-1} is calculated from the following equation:

$$\tau_{NP}^{-1} = v_s \left[\left(2\pi R_{NP}^2\right)^{-1} + \left(\pi R_{NP}^2 \frac{4}{9} \left(\frac{\Delta\rho}{\rho} \right)^2 \left(\frac{x k_B T R_{NP}}{\hbar v_s} \right)^4 \right)^{-1} \right]^{-1} N_{NP} \quad (9)$$

Dislocation scattering that includes both dislocation core (τ_{DC}^{-1}) and dislocation strain (τ_{DS}^{-1}) scattering.

$$\tau_{DC}^{-1} = N_D \frac{V_s^{4/3}}{v_s^2} \omega^3 \quad (10)$$

$$\tau_{DS}^{-1} = A' N_D \gamma^2 B_D^2 \omega \left\{ \frac{1}{2} + \frac{1}{24} \left(\frac{1-2v_s}{1-v_s} \right)^2 \left[1 + \sqrt{2} \left(\frac{v_L}{v_T} \right)^2 \right]^2 \right\} \quad (11)$$

Detailed parameters are shown in Table S2.

Density functional theory calculations

Density functional theory calculations were performed using the projector augmented wave (PAW) method, as implemented in the Vienna Ab initio Simulation Package (VASP)[1-2], with the Perdew, Burke, and Ernzerhof (PBE)[3] generalized gradient approximation (GGA) utilized for the exchange-correlation energy functional. A 2×2×3 supercell of PbSe (60 atoms) is adopted. The pristine PbSe, and Cu doped cell (PbSeCu) are fully relaxed individually with A 8×8×4 Γ-centered Monkhorst-Pack k-point mesh and a plane-wave cutoff energy of 450 eV

until the forces on atoms were smaller than 1×10^{-2} eV/Å. The energy convergence criterion of 10^{-6} eV were employed for all calculations. The van der Waals interaction is taken into account in DFT-D2 method as implemented in VASP. In the calculation of density of sate (DOS), a denser k-point mesh (10×10×6) is adopted.

For the calculations of charged defect formation energy, we used the following formula:

$$E_f = E(\text{defect, q}) - E(pure) - \sum_i n_i\mu_i + q\,(E_V + E_F + \Delta V)$$

$E(\text{defect, q})$ and $E(\text{pure})$ are the total energies of unit cells with and without defect separately. $n_i\mu_i$ is the reference energy of n_i added atoms of element *i* with chemical potential μ_i. E_V is the valence band maximum, E_F is the Fermi level position, and ΔV is the core level correction.

3. Supplementary Figures

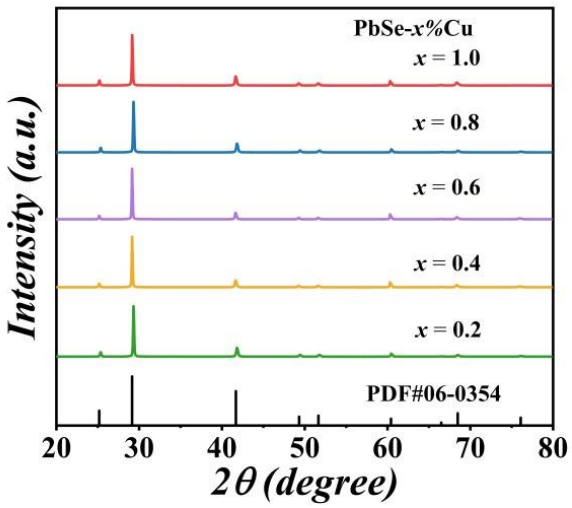

Figure S1. The powder X-ray diffraction patterns for the PbSe-*x*%Cu (*x* = 0.2, 0.4, 0.6, 0.8, 1.0) samples.

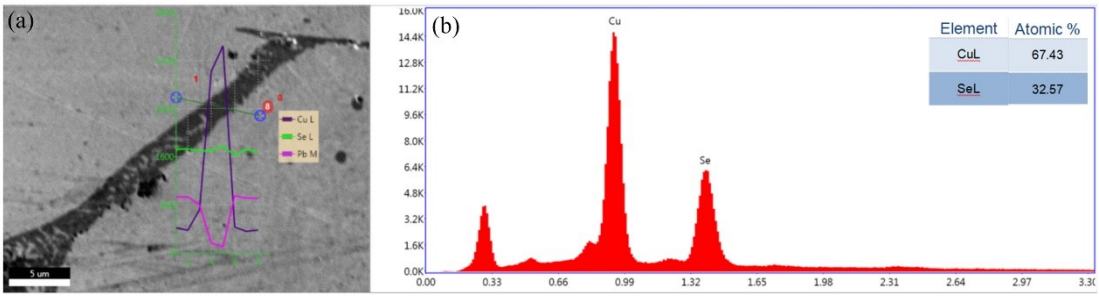

Figure S2. The line scan for the PbSe-4%Cu_2Se samples.

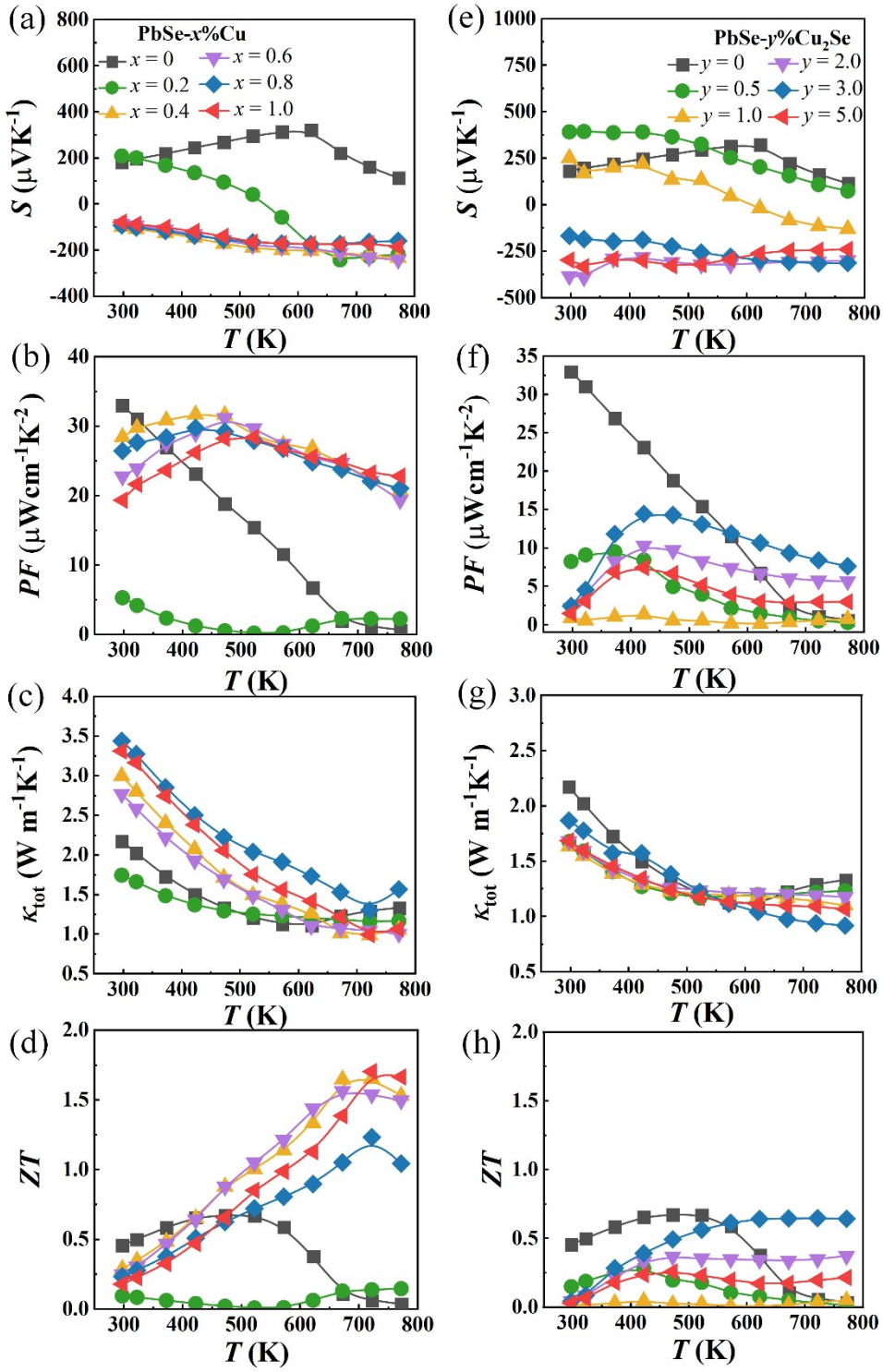

Figure S3. Temperature-dependent thermoelectric properties of PbSe-*x*%Cu (*x* = 0, 0.2, 0.4, 0.6, 0.8, 1.0): (a) Seebeck coefficient; (b) power factor; (c) total thermal conductivity; (d) *ZT* values. Temperature-dependent thermoelectric transport properties in PbSe-*y*%Cu_2Se (*y* = 0, 0.5, 1.0, 2.0, 3.0, 5.0): (e) Seebeck coefficient; (f) power factor; (g) total thermal conductivity; (h) *ZT* values

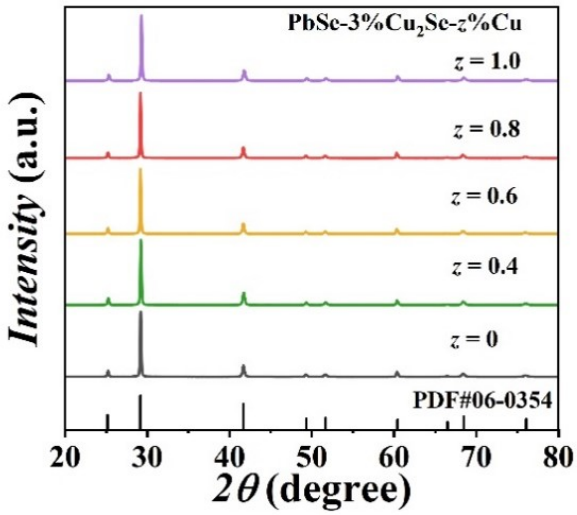

Figure S4. The powder X-ray diffraction patterns for the PbSe-3%Cu_2Se-*z*%Cu (*z* = 0, 0.4, 0.6, 0.8, 1.0) samples.

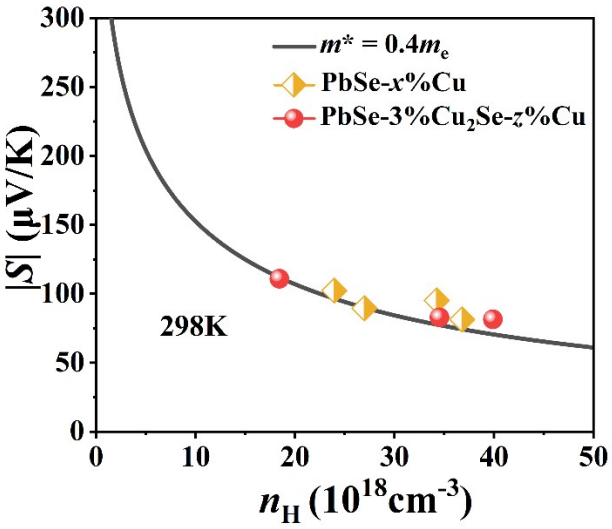

Figure S5. Calculated Pisarenko line using SPB model[4] versus data of PbSe-x%Cu (x = 0.4, 0.6, 0.8, 1.0) and PbSe-3%Cu_2Se-z%Cu (z = 0.6, 0.8, 1.0) samples.

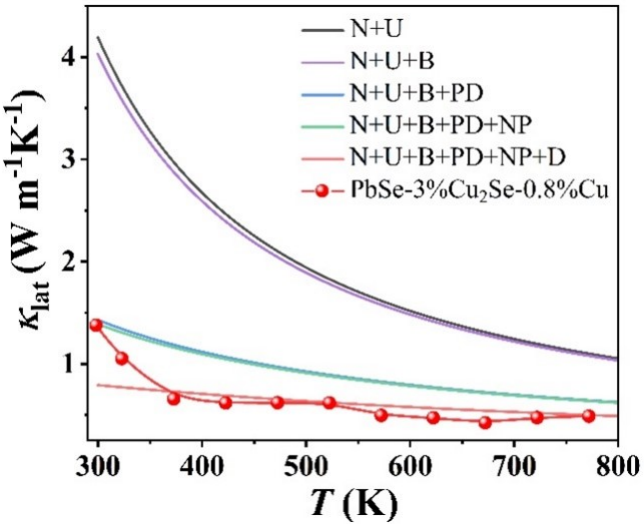

Figure S6. Fitting of temperature-dependent lattice thermal conductivity κ_{lat} of the PbSe-3%Cu_2Se-0.8%Cu sample using Debye-Callaway model by considering Umklapp phonon-phonon scattering (*U*), normal phonon-phonon scattering (*N*), boundary scattering (*B*), point defect scattering (*PD*), nanoprecipitates (*ND*) and dislocation (*D*) processes.

3. Supplementary Tables

Table S1. Dopant concentrations and corresponding carrier densities for PbSe-3%Cu_2Se-*z*%Cu at room temperature.

PbSe-3%Cu_2Se-*z*%Cu				
z	**0**	**0.6**	**0.8**	**1.0**
n **(10^{18} cm^{-3})**	0.214	18.469	34.602	39.973

Table S2. Parameters for the Debye-Callaway model.

Paramaters	symbol	values	Ref
Average atomic mass (kg)	M_{av}	2.37556×10^{-25}	experiments
Average atomic mass volume(kg)	V_{av}	2.87229×10^{-29}	experiments
Boltzmann constant (J/K)	k_B	1.38×10^{-23}	/
Grüneisen parameter	γ	1.7393	5
Average sound velocity (m/s)	v_s	2335.4	6
Longitudinal velocity (m/s)	v_L	3150	6
Transverse velocity (m/s)	v_T	1700	6
Debye temperature (K)	θ_a	180.2	experiments
Umklapp to normal ratio	B_N	4	7
Pre-factor for dislocation scattering	A'	0.96	8
Poisson ratio	r	0.243	7
Phenomenological parameter	ε	64	9
Burgers vector (m)	B_D	4.33×10^{-10}	6
Dislocation density(m^{-2})	N_D	4×10^{11}	experiments
Number density of nano-precipitates (m^{-3})	N_{NP}	2.8×10^{18}	experiments
Radius for the nano-precipitates (m)	R_{NP}	104.4031×10^{-9}	experiments
Matrix density ($g\cdot cm^{-3}$)	ρ	8.2	experiments
Density difference between matrix and precipitates ($g\cdot cm^{-3}$)	$\Delta\rho$	0.7	experiments
Characteristic of the vibrational	b	0.9	/
Grain size (m)	D	4×10^{-6}	experiments
Disorder scattering parameter	Γ	0.200830266	experiments

References

1. B. Jia, Y. Huang , Y. Wang, Y. Zhou, X. Zhao, S. Ning, X. Xu, P Lin, Z. Chen, B. Jiang and J. He, *Energy Environ*. *Sci*., 2022, **15**, 1920-1929.
2. G. Kresse and D. Joubert, *Phys. Rev. B*, 1999, **59**, 1758.
3. J. Sun, R. Wang, W. Cui, S. Xie, T. Luo, H. Bai, X. Zhao, Z. Chen, X. Sang, X. Tan, X. Tang and G. Tan, *Chem. Mater.* 2022, **34**, 6450-6459.
4. R. Marlow, S. Kuriyakose, N. Mesaros, H. H. Han, R. Tomlinson, S. N.Faust, M. D. Snape and A. J. Pollard, A. Finn, *Vaccine* 2018, **36**, 2300-2306.
5. J. Sun, C. Xie, W. Cui, F. Yan, J. Li, J. Zhang, X. Sang, X. Tang and G.Tan, *Chem. Mater.*, 2023, **35**, 4366-4374.
6. Z. Chen, B. Ge, W. Li, S. Lin, J. Shen, Y. Chang, R. Hanus, G. J. Snyder and Y. Pei, *Nat. Commun*., 2017, **8**, 13828.
7. H. Wang, Y. Pei, A. D. LaLonde and G. J. Snyder, *Proc. Natl. Acad. Sci.*, 2012, **109**, 9705-9709.
8. W. R. G. Kemp, P. G. Klemens and R. J. Tainsh, *Philos. Mag.*, 1959, **4**, 845-857.
9. H. Wang, J. Wang, X. Cao and G. J. Snyder, *J. Mater. Chem. A*, 2014, **2**, 3169-3174.